https://doi.org/10.5194/egusphere-2026-3758
Preprint. Discussion started: 20 August 2026

Evaluating European Ground Motion Service against Local InSAR Analysis along Key Swedish Corridors

Saeid Aminjafari[1,2], Faramarz Nilfouroushan[3,4], Frida Carlvik[5], Mehdi Darvishi[3], Leif E.B. Eriksson[1]

[1]Department of Environmental and Energy Sciences, Chalmers University of Technology, Gothenburg, 41296 Sweden
[2]Department of Physical Geography and Bolin Centre for Climate Research, Stockholm University, Stockholm, 10691 Sweden
[3]Department of Computer and Geospatial Sciences, University of Gävle, 80176 Sweden
[4]Department of Geodetic Infrastructure, Lantmäteriet, Gävle, 80264 Sweden
[5]Department of Technology and Society, Lund University, Lund, 22100 Sweden

Correspondence to: Saeid Aminjafari (saeid.aminjafari@chalmers.se)

Abstract. Ground motion poses a significant threat to the safety and functionality of transport infrastructure, particularly in regions affected by landslides, subsidence, freeze–thaw processes, and large-scale tunnelling. Interferometric Synthetic Aperture Radar (InSAR) enables millimetre-level displacement monitoring over large areas and is used to support infrastructure risk assessment. Here, we evaluate the usability of two InSAR approaches, (i) Persistent Scatterer Interferometry (PSI) using displacement products from the European Ground Motion Service (EGMS), and (ii) a combined Persistent- and Distributed-Scatterer (PS+DS) phase-linking workflow across key Swedish transport corridors. Rather than a strictly controlled methodological comparison, we evaluate how differences between operational InSAR solutions translate into practical performance for infrastructure monitoring. Results show that PS+DS consistently yields five times as many measurement points while maintaining RMSE values within a similar range to EGMS (mostly below 6 mm in the Line Of Sight direction). The EGMS exhibits narrower RMSE distributions, but PS+DS achieves comparable median RMSE of the measurement points across most land-cover types and corridor environments. Both datasets capture similar displacement patterns along all corridors, with measurement points from both approaches concentrating within the linear corridor geometry. Overall, the five-fold increase in PS+DS point density offers infrastructure operators a practical pathway to finer-scale ground motion monitoring for railway maintenance and risk assessment, while demonstrating how the choice of operational InSAR processing strategy shapes the information available for Earth-observation-based infrastructure applications.

1 Introduction

Linear infrastructure forms the backbone of society and its uninterrupted functioning supports economic stability, regional connectivity, and public safety (Johnsson and Balstrøm, 2021). Yet, these networks are vulnerable to ground motion driven by a range of geophysical and hydro-climatic processes. Landslides, land subsidence, permafrost dynamics, embankment failures, and soil erosion can all compromise the structural integrity of transport corridors (Koks et al., 2019). When such

https://doi.org/10.5194/egusphere-2026-3758
Preprint. Discussion started: 20 August 2026

processes are not detected or mitigated in time, the consequences can be severe, e.g., train derailments, road collapses, traffic accidents, service disruptions, and substantial human and financial losses (Johnsson and Balstrøm, 2021; Koks et al., 2019). Sweden has undergone several recent and concerning examples, including a passenger train derailment due to over-saturated soil, repeated disruptions on the Iron Ore Line (i.e., Malmbanan, which transports 90% of the EU's iron ore supply) linked to heavily stressed infrastructure, and a major landslide that destroyed part of the E6 highway (SHK, 2024, 2025a, b). Given these risks, systematic monitoring of ground motion around linear infrastructure is essential, as early detection can enable targeted maintenance, risk mitigation, and informed decision-making.

Interferometric Synthetic Aperture Radar (InSAR) is uniquely suited for this task (Azadnejad et al., 2025; Banic et al., 2025; Piter et al., 2024). Unlike geodetic field surveys and GNSS, which provide sparse point measurements, InSAR offers spatially continuous displacement fields with millimeter-level precision (Aziz Zanjani et al., 2024; Sadhasivam et al., 2025). It operates at low cost, in all weather conditions, day and night, and has been successfully applied in numerous studies focusing on railways, highways, pipelines, embankments, and subsidence zones (Azadnejad et al., 2024; Yang et al., 2025).

To date, three main InSAR time series approaches have been developed which offer complementary advantages: Persistent Scatterer Interferometry (PSI), Small BAseline Subset (SBAS), and combined Persistent and Distributed Scatterer (PS+DS). PSI extracts long-lived radar scatterers from built structures, making it particularly effective for railway monitoring (Ferretti et al., 2001, 2011; Kotzerke et al., 2022). The European Ground Motion Service (EGMS), funded by the European Commission, provides InSAR estimates over Europe from full-resolution Copernicus Sentinel-1 SAR data and relies primarily on PSI for its continental-scale products (Crosetto et al., 2026) and Distributed Scatterer (DS) for limited specific regions (Costantini et al., 2021; Crosetto et al., 2021; Ferretti et al., 2025; Kotzerke et al., 2022). Here, we use EGMS Calibrated product, with GNSS-referenced, continent-wide harmonised LOS displacement time series, which is explicitly described as suitable for linear infrastructure monitoring (Kotzerke et al., 2022), hereafter referred to as EGMS-PS.

By contrast, InSAR solutions using only Distributed Scatterer (DS) average phase across multiple pixels and are better suited for broad-scale terrain motion, landslides, ground subsidence, or regional uplift/subsidence (Berardino et al., 2002), and generally provide faster processing with wider spatial coverage but lack the targeted point-level precision needed for narrow transport corridors (Yunjun et al., 2019).

PS+DS hybrid methods combine the stability of PS with the higher point density of DS through phase linking, which tackle decorrelation noise by forming all possible interferometric pairs in a SAR data stack, and routinely produce significantly higher point densities in natural terrain at the cost of more complex processing workflows (Ansari et al., 2018; Ferretti et al., 2011; Mirzaee et al., 2023; Piter et al., 2024; Staniewicz et al., 2025, 2024).

The key question addressed here is whether publicly available products such as EGMS-PS are sufficient for railway corridor monitoring, or whether additional investment in locally processed InSAR workflows is warranted. In this context, the aim of this study is not to establish a strictly controlled comparison between processing methods, which may differ fundamentally in their underlying assumptions, metrics, and implementations, but rather to evaluate how these operational solutions translate into practical outcomes such as spatial coverage, uncertainty, and the ability to capture deformation patterns along

https://doi.org/10.5194/egusphere-2026-3758
Preprint. Discussion started: 20 August 2026

linear infrastructure. We examine point count, residual errors of the displacements over the time series (i.e., RMSE; refer to (Kotzerke et al., 2022)), short-range velocity variability, distance of measurement points to the infrastructure centreline, potential geolocation and DEM-related effects, and the influence of land cover on these metrics across five Swedish transport corridors with known or suspected deformation drivers including freeze–thaw dynamics, landslides, and underground excavation.

2 Methods and materials

2.1 Study area

We selected five representative case studies to evaluate InSAR performance along Swedish transport corridors (Fig. 1), spanning a range of displacement drivers, climatic zones, land-cover types, and infrastructure characteristics. Because the two methods behave consistently across all five corridors, we present two representative cases in detail in the main text and provide the corresponding figures for the remaining three cases, which show the same patterns, in the supplementary.

Case 1: E45 highway and the regional railway in Lilla Edet city (southwest Sweden): this case covers a ~5.5 km × 5 km area southwest of Lake Vänern, including a 5 km section of the E45 highway and a regional railway line. Land cover consists of a mixture of agricultural land, forest, and urban zones. This area lies within a region historically prone to landslides and rapid ground motion (SHK, 2025b), providing conditions suitable for testing InSAR sensitivity to climate-induced and geotechnical instability.

Case 2: The West Link (Västlänken) in Gothenburg city is an urban underground railway corridor in central Gothenburg. The West Link consists of approximately 6 km of tunnel and 2 km of above-ground track. Ground motion in densely built urban settings, where radar visibility, scattering conditions, and construction-related displacement are highly variable, provides an opportunity to assess point count and consistency under PS- and DS-dominant scattering environments. The corridor is partially under construction during the study period and early surface responses to the tunnel project may be present, however, investigating construction-induced surface displacement is beyond the scope of this study. Analysis was performed within a 100 m-wide corridor centered on the underground alignment.

The remaining three cases, Malmbanan railway / E10 highway (northern Sweden with strong seasonal temperature gradients), a second southwest Swedish corridor (landslide prone area), and the E4 Stockholm Bypass (Förbifart Stockholm, underground construction) follow the same evaluation framework and are described in the supplementary material.

https://doi.org/10.5194/egusphere-2026-3758
Preprint. Discussion started: 20 August 2026

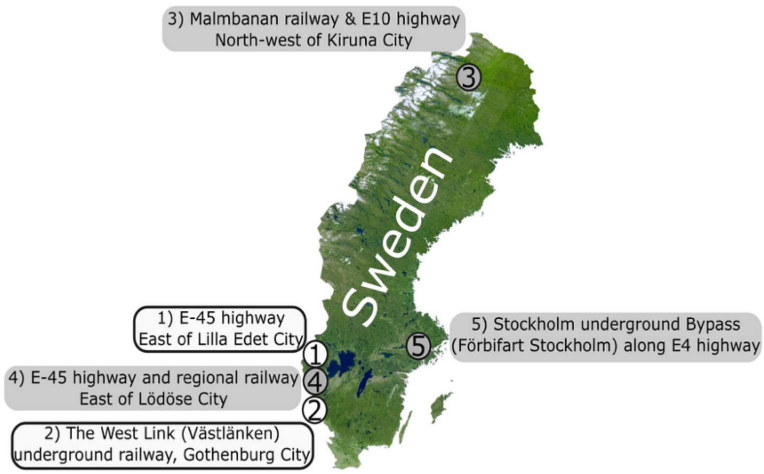

Figure 1. Geographic location of the five study areas across Sweden. Cases 1 and 2 (white boxes) are presented in the main text and Cases 3–5 (gray boxes) are detailed in the supplementary material.

2.2 Theory: Persistent scatterer interferometry

InSAR derives displacement by comparing two SAR images acquired at different times, with the resulting phase difference reflecting changes in satellite–target distance. The interferometric phase also contains contributions from topography, atmospheric delays, and noise, which different InSAR methods model and separate to isolate the ground-motion signal (Aminjafari et al., 2024). PSI identifies a sparse network of radar targets whose backscattered signal remains stable over long temporal and geometric baselines, selected using the amplitude dispersion index (Da = standard deviation / mean amplitude), where low values (typically Da ≤ 0.25) indicate temporally stable reflectors. PSI exploits a multi-interferogram framework to jointly estimate DEM errors, displacement rates, and atmospheric phase delays across all acquisitions, enabling millimeter-level velocity precision even where conventional interferograms decorrelate (Ferretti et al., 2001). The EGMS adopts these core PSI principles (Ferretti et al., 2001) together with advanced algorithms such as SqueeSAR (Ferretti et al., 2011) with flexible displacement modelling including non-linear and seasonal motion components for operational continental-scale monitoring (Costantini et al., 2021). In the EGMS dataset, every measurement point has an attribute named "mp_type", with 0 values being PS and non-zero values being DS (Costantini et al., 2021). The EGMS subset in Sweden does not cover any DSs, meaning that "mp_type" is zero for all measurement points in our subset in Sweden.

2.3 Theory: combined PS and DS interferometry

2.3.1 Phase linking

For DS processing, we adopt the non-linear phase linking framework of Mirzaee et al. (2023), implemented in the MiaplPy package, which estimates an optimal wrapped phase time series from the full stack of coregistered single-look complex (SLC) images. Pixels are first grouped into statistically homogeneous neighbourhoods (SHP) using a two-sample

https://doi.org/10.5194/egusphere-2026-3758
Preprint. Discussion started: 20 August 2026

Kolmogorov-Smirnov test, and their complex values are averaged to form a covariance matrix C of size N × N for a stack of N SLC images, where each element $C_{i,j} = \langle s_i \times s_j^* \rangle$ represents the interferometric product between acquisitions i and j. From the covariance matrix, one can derive the coherence matrix, whose elements are normalized:

$$\gamma_{i,j} = C_{i,j} \Big/ \sqrt{C_{i,i} \times C_{j,j}} \qquad (1)$$

The elements of the covariance matrix describe how strongly every pair of SAR acquisitions is related. Phase linking uses the full covariance structure to retrieve the most likely wrapped phase history. We adopt a combined approach introduced by Mirzaee et al. (2023): the Eigenvalue decomposition-based Maximum likelihood of Interferometric phase (EMI) framework (Ansari et al., 2018) is used as the primary estimator, with classical Eigenvalue Decomposition (EVD) as a fallback when the coherence matrix is not invertible (Mirzaee et al., 2023; Staniewicz et al., 2025). Only DSs with a goodness-of-fit ≥ 70% between the phase-linked and primary phase values are retained (Piter et al., 2024).

To reduce computational load on large Sentinel-1 stacks, MiaplPy implements phase linking sequentially: the SLC archive is divided into mini-stacks, each phase-linked independently and compressed into a synthetic SLC before being appended to the next mini-stack (Ansari et al., 2017, 2018; Mirzaee et al., 2023; Staniewicz et al., 2025).

2.3.2 PS and DS selection

After phase linking, we follow the SARvey package framework by Piter et al. (2024) for pixel selection and time-series inversion. PSs are identified using a combination of low amplitude dispersion (Da ≤ 0.42, see Mirzaee et al. (2023)), low wrapped phase noise (high SNR), and top eigenvalue percentage of the coherence matrix (≥ 95%, see Piter et al. (2024)), while DSs are identified via the phase-linking process. Phase noise is estimated using temporal coherence method, which approximates spatially correlated phase contributions through a neighbourhood filter and computes residuals relative to the local mean across all interferograms, yielding a temporal coherence value between zero and one corresponding to the lowest and the highest SNR respectively (Piter et al., 2024).

2.3.3 Time series retrieval

The SARvey package implements a two-step approach to retrieve displacement time series (Piter et al., 2024). In the first step, high-quality first-order points (temporal coherence ≥ 0.9) form a stable spatial network via Delaunay triangulation, from which DEM errors and velocity differences are estimated using double-differenced phases and weighted least squares. Atmospheric effects are estimated from residuals using Kriging, assuming spatial correlation but temporal independence. In the second step, second-order points (temporal coherence ≥ 0.7) including both PS and DS are added, the estimated atmospheric phase is removed from their wrapped phases, and displacement time series are retrieved through the same unwrapping and network inversion procedure. Because no temporal model is imposed, both linear and non-linear displacements can be retrieved.

2.4 Evaluation

To evaluate PS ground motion time series and velocities in the LOS direction obtained from EGMS-PS against the phase-linking PS+DS pipeline, we apply consistent amplitude dispersion (Da ≤ 0.42) and temporal coherence (≥ 0.7) thresholds to both datasets, recognising that the underlying quality metrics are not identical across processing chains. We assess point count, displacement residual errors (RMSE), short-range velocity variability, distance of measurement points to the infrastructure centreline, potential geolocation and DEM-related effects, and land-cover influence on these metrics. RMSE is computed from the variation of displacement over the time series (in mm) and serves as a measure of displacement precision, following the EGMS documentation (Kotzerke et al., 2022).

2.5 Data

Copernicus Sentinel-1 SAR images for PS+DS processing were acquired from the NASA Alaska Satellite Facility Distributed Active Archive Center (ASF DAAC) operated by the University of Alaska Fairbanks (UAF), covering the period 2020–2024. Topographic phase was removed using the 30 m Copernicus Global DEM (Copernicus DEM - Global and European Digital Elevation Model | Copernicus Data Space Ecosystem, 2025). EGMS Calibrated product data in the LOS direction were downloaded from the EGMS platform clipped to the PS+DS processing extent and filtered using the thresholds described in Sect. 2.4. The EGMS subset in Sweden does not cover any DSs.

Ascending orbit data were used for the three non-urban corridors, and descending orbit data were used for the Gothenburg and Stockholm cases. Winter acquisitions were excluded from the locally processed time series to match the reduced winter coverage of the EGMS Calibrated product, ensuring a consistent set of acquisition dates across both datasets.

Land cover analysis used the 10 m Swedish National Land Cover Database (NMD 2023) provided by the Swedish Environmental Protection Agency via space and airborne data. Transport network geometry was obtained from the Swedish mapping, cadastral and land registration authority (Lantmäteriet).

3 Results and discussion

3.1 LOS velocity maps of transport corridors

The LOS velocity maps derived from both EGMS-PS and the PS+DS phase-linking approach reveal generally slow ground-motion signals across the investigated corridors, with localized zones of subsidence in the case studies (Fig. 2).

In Case 1, Lilla Edet, both EGMS-PS and PS+DS identify a rapidly subsiding zone along the E45 highway and in areas west of the road, with velocities exceeding 5 mm/year (Fig. 2a-b). The consistency of this signal across both methods suggests a regional displacement pattern rather than a method-specific artifact, likely related to local geological or geotechnical conditions.

https://doi.org/10.5194/egusphere-2026-3758
Preprint. Discussion started: 20 August 2026

For Case 2, the West Link (underground railway in Gothenburg), localized subsidence of approximately 5 mm/year is detected near the northern and southern ends of the tunnel alignment (Fig. s 2c-d). These signals are more clearly expressed in the PS+DS velocity maps, particularly in sections associated with above-ground construction activity. These localized tunnel-corridor signals resemble construction-related subsidence patterns reported, by Aziz Zanjani et al. (2024), which showed that InSAR can capture localized settlement from large-scale construction when combined with contextual information such as construction timelines and geotechnical data.

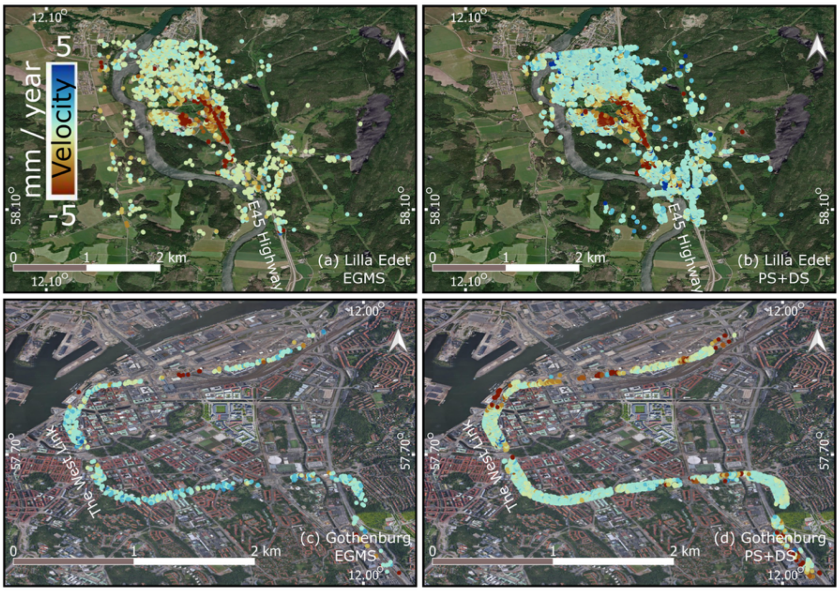

Figure 2. The ground motion velocity maps between 2020 and 2024 from the EGMS-PS Calibrated LOS product on the left column, and from the PS+DS approach on the right column, (a-b) E-45 highway, east of Lilla Edet City, (c-d) The West Link (Västlänken) underground railway, Gothenburg City. The basemap for panels a-b was designed and developed by Esri, Sources: Esri, Maxar, GeoEye, Earthstar Geographics, CNES/Airbus DS, USDA, USGS, AeroGRID, IGN, and the GIS User Community | Powered by Esri. The basemap for panels c-d: Imagery © 2026 NASA, Map data © 2026 Google.

3.2 Velocity change and point count along corridors

Rather than focusing on individual scatterers, we compute summary statistics of the scatterer populations within each 100 m chainage segment, providing a more robust basis for evaluation. Across all case studies, the velocity profiles show that EGMS-PS and PS+DS produce broadly similar displacement patterns, despite differences in point count (Fig. 3).

In Lilla Edet (E45 highway), both methods detect similar subsidence rates of ~8 mm/year in the middle of the corridor (Fig. 3a-b), highlighting a section that may warrant attention from the Swedish Transport Administration. Along the West Link corridor in Gothenburg, both methods reveal localized subsidence of about 5 mm/year near the 12th and 70th chainage segments (Fig. 3c-d).

The point count of EGMS-PS decreases sharply across all study corridors and their surrounding areas compared to PS+DS, which yields consistently denser and more spatially continuous measurements both along the linear infrastructure and in the broader landscape (grey bars in Fig. 3 and heatmaps in Fig. S3). Locations with higher point count generally exhibit lower

https://doi.org/10.5194/egusphere-2026-3758
Preprint. Discussion started: 20 August 2026

RMSE, indicating that measurement redundancy improves displacement quality (Fig. 3). In contrast, there is no clear relationship between RMSE and the magnitude of velocity variations, suggesting that even abrupt displacement is captured with acceptable residual errors by both methods.

This point-count contrast is consistent with previous infrastructure-focused InSAR studies (Piter et al., 2024; Wu et al., 2026): PSI approaches provide highly stable measurements over man-made structures but suffer fragmented coverage in vegetated or mixed terrain, whereas DS-capable methods improve spatial continuity across both built and vegetated environments without compromising precision (Wu et al., 2026). Consistently, Aziz Zanjani et al. (2024) report that at national and local scales PS+DS yields significantly higher point counts along man-made infrastructure, while PSI provides a sparser but more conservative displacement field.

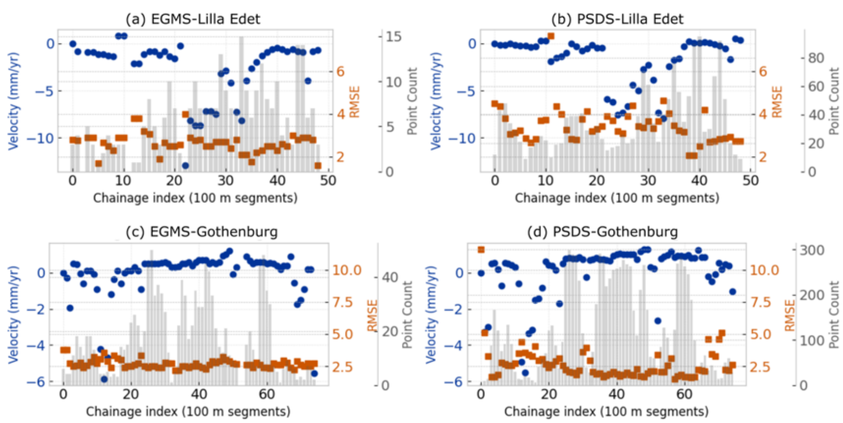

Figure 3. Summary statistics (median) of velocity and displacement RMSE every 100 m chainage along the corridors, with EGMS-PS (left panels) and PS+DS (right panels). Left axes show LOS velocity referenced to the first chainage; right axes show RMSE (mm), with grey bars indicating point counts.

3.3 Residual errors (RMSE) and velocity distributions

While higher point count is often desirable, it does not automatically translate into better information, since additional points may include low-quality or noisy measurements. To assess the reliability of both methods, we compute and analyse their RMSE, which reflects the precision of the displacement for each measurement point (Kotzerke et al., 2022). Overall, RMSE values of both EGMS-PS and PS+DS fall within a relatively narrow range up to ~6 mm in the LOS direction across all case studies (Fig. 4 and Fig. S4).

The cumulative probability curves for RMSE show that EGMS-PS exhibits consistently steeper distributions than PS+DS, indicating a higher proportion of low-RMSE points in the EGMS-PS data (Fig. 4, left panels). Nonetheless, a substantial share of PS+DS points (≥ 50 %) achieve RMSE values comparable to EGMS-PS despite the much larger PS+DS point count: in Lilla Edet the RMSE for half the points is similar for both methods at roughly 3 mm, in the Gothenburg corridor the 80th percentile corresponds to approximately 3 mm (Fig. 4, left panels, and Fig. S5). A small number of segments with comparatively high PS+DS RMSE (up to ~11 mm), particularly in the Gothenburg tunnel sections, may reflect increased

https://doi.org/10.5194/egusphere-2026-3758
Preprint. Discussion started: 20 August 2026

short-term variability from decorrelation, atmospheric effects, or localized non-linear motion in dense urban environments; as these cases are limited and introduce no systematic velocity bias, they are unlikely to affect the corridor-scale comparisons or main conclusions.

For velocity, the cumulative probability curves of both methods are similarly steep across all case studies (Fig. 4, right panels and Fig. S5), although the PS+DS curves exhibit slightly longer tails towards higher velocities, suggesting a few locations with comparatively large displacement rates. Such occasional higher-magnitude velocities have been linked to decorrelation, vegetation dynamics, and soil-moisture variability, which can increase phase bias and uncertainty when network design and coherence thresholds are not adapted to land-cover conditions (Karami et al., 2025). While these may represent genuine localized motion, their interpretation requires caution. Moreover, Li et al. (2026) recommend treating InSAR velocities below 5 mm yr^{-1} with particular care given InSAR's difficulties in vegetated terrain.

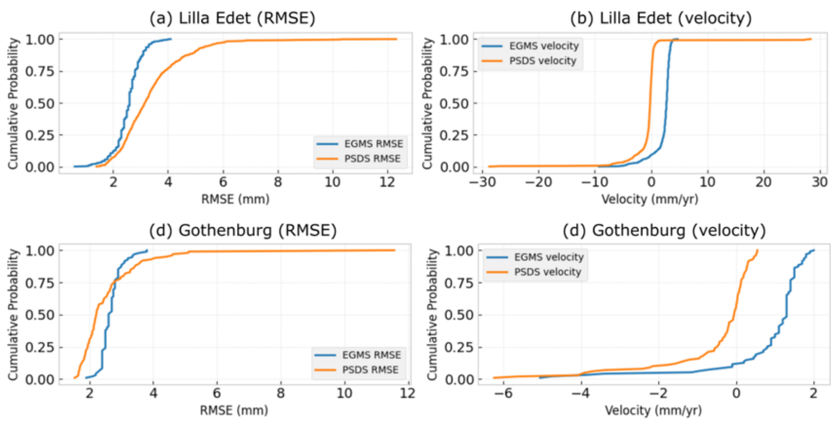

Figure 4. Cumulative probability distributions of RMSE (left panels) and velocity (right panels) for the EGMS-PS and PS+DS. Both values are medians within 100 m × 100 m grid cells.

To account for unequal sampling along the corridors, we recomputed corridor-level RMSE and velocity by weighting each 100 m chainage segment by its point count (Fig. S6). Under this weighting, the RMSE curves for EGMS-PS and PS+DS become similarly steep (Fig. S6, left panels), because segments with many PS+DS points exert greater influence and a substantial fraction of these points also exhibit low RMSE. Thus, the higher PS+DS point count does not introduce additional noise but includes many observations of quality comparable to EGMS-PS. The weighted velocity distributions remain similarly steep for both methods (Fig. S6, right panels), confirming that both capture slow, smoothly varying displacement along the corridors. This redundancy effect, corridor segments with higher point count exhibiting lower RMSE, has also been reported in earlier DS-based infrastructure studies, where dense sampling stabilised aggregated displacement estimates even when individual measurements showed higher variance (Aziz Zanjani et al., 2024). Differences in atmospheric phase mitigation between the two data-driven processing chains may also contribute to the observed RMSE variations (Ferretti et al., 2025; Piter et al., 2024) although given the small spatial extent of our study areas such large-scale corrections are expected to have limited influence. Finally, the methods differ in displacement modelling: seasonal signals

https://doi.org/10.5194/egusphere-2026-3758
Preprint. Discussion started: 20 August 2026

(e.g., thermal expansion) are present but not explicitly modelled in the SARvey inversion (Piter et al., 2024), whereas EGMS incorporates seasonal components in its polynomial temporal model, allowing clearer separation between trends and periodic deformation (Ferretti et al., 2025).

3.4 Performance in different land covers

The RMSE boxplots across land-cover classes show that EGMS-PS values vary within a narrower range with fewer large values, whereas PS+DS displays a wider spread but generally exhibits equal or lower median RMSE for most land-cover types across all case studies (Fig. 5, left panels). This indicates that PS+DS captures more RMSE variability, as expected from the inclusion of DS pixels, yet maintains comparable or better central accuracy. Land-cover type does not appear to strongly influence RMSE, contrary to the expectation that agricultural or vegetated areas would yield higher errors.
EGMS-PS contains a higher proportion of points in built-up areas, roads, and railways, consistent with the PS-only selection over Sweden, and a lower proportion in vegetated or non-urban terrain than PS+DS (Fig. 5, right panels). In absolute terms, however, PS+DS yields approximately five times more measurement points across all land-cover classes, including built-up areas and transport infrastructure.

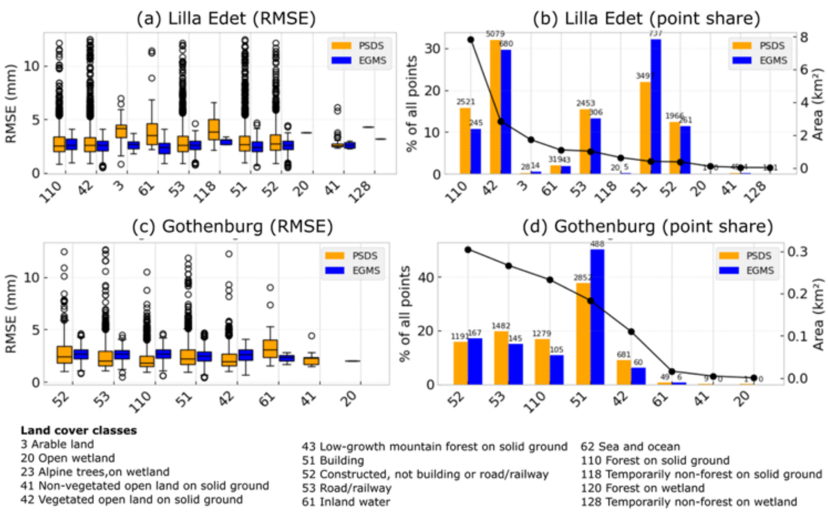

Figure 5. Left panels: RMSE boxplots for EGMS-PS and PS+DS across land-cover classes. Right panels: point-percentage (left axis) and land-cover area (right axis). The numbers on top of bars are the number of measurement points. Points appearing over water bodies originate from bridges, near-shore pixels, or sidelobes of onshore scatterers.

3.5 Closeness to the corridor

The distance-to-centreline analysis provides insight into how each method spatially aligns with the transport infrastructure, without implying absolute geolocation accuracy. All measurement points were clipped to a 20 m corridor around every mapped road and railway segment (including local streets), and point proportions were computed within distance bins relative to the centreline.

https://doi.org/10.5194/egusphere-2026-3758
Preprint. Discussion started: 20 August 2026

Both methods identify similar proportions of points close to road centrelines, with approximately 20–30% within 0–5 m and 40–50% within 5–10 m across all case studies (Fig. 6, left panels and Fig. S8). For railways, differences between methods are small and not systematic: PS+DS detects slightly more points near the track in Lilla Edet and Gothenburg (Fig. 6, left panels), but these should not be interpreted as evidence of consistent lateral offsets. The distance boxplots reinforce this: for roads, the median and overall distribution of distances to the centreline are nearly identical for both methods, while for railways PS+DS shows lower medians (closer distances to the centerline) in Lilla Edet but without a clear systematic pattern across cases (Fig. 6, right panels and Fig. S8). Roads show substantially higher point counts than railways due to their larger corridor width, whereas railway measurements cluster more tightly around the centreline.

Scatter plots of RMSE and elevation (DEM) against distance to centreline can reveal geometry-related patterns in some cases (Fig. S9–S10). A weak signal appears in Lilla Edet, where EGMS-PS shows a negative RMSE–distance correlation and a positive DEM–distance correlation for the railway, indicating that points farther than ~5 m from the track tend to lie at different elevations and are unlikely to belong to the railway structure, a behaviour useful for assessing measurement point geolocation (Aziz Zanjani et al., 2024). However, for the case of Gothenburg, due to the low relief, there is no notable correlations, likely because the flat topography does not separate the corridor from its surroundings (Fig. S9–S10).

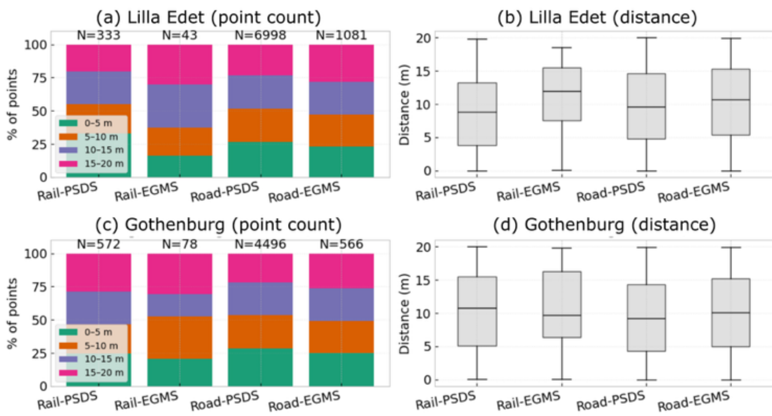

Figure 6. Left panels: stacked bar charts showing the percentage of points within 0–5, 5–10, 10–15, and 15–20 m of road and railway centreline, based on data clipped to a 20 m corridor around all transport segments. The numbers on top of bars are the number of measurement points. Right panels: boxplots of distance to centreline.

3.6 Why identical numeric thresholds do not impose equivalent filtering

To assess how processing choices affect the comparison between EGMS and locally processed InSAR, we excluded DSs from our chain (hereafter locally processed PS) and ran a sensitivity analysis for the Lödöse corridor across temporal coherence thresholds of 0.7, 0.5, and 0.3 (Fig. S11–S13). Relaxing the temporal coherence threshold raised point count substantially for PS+DS, moderately for locally processed PS, and only marginally for EGMS-PS, indicating that EGMS selection is governed by additional constraints such as amplitude dispersion, so a common numeric threshold of temporal coherence does not impose equivalent filtering across chains (Fig. S11). Moreover, the RMSE remained lowest for EGMS-

PS and increased modestly for the locally processed InSAR as the temporal coherence threshold relaxed, mostly in non-urban areas, though the overall range stayed low (Fig. S12). Velocity patterns along the railway were broadly consistent across methods at different temporal coherence thresholds, with EGMS-PS the most spatially stable and PS-based local results more variable at lower thresholds (Fig. S13). These differences are not only due to different point selection strategies but also differing stack designs, seasonal decorrelation, unwrapping strategies, and EGMS's sparse coherent-network approach versus SARvey's first/second-order densification (Ferretti et al., 2025; Piter et al., 2024). The sensitivity of derived rates to coherence-threshold choice echoes Li et al. (2026), who likewise find that filtering and coherence-related processing choices can substantially alter InSAR-derived rates in low-coherence settings.

4. Conclusion

This study evaluated displacement products from EGMS-PS against a phase-linked combined Persistent and Distributed Scatterer (PS+DS) workflow along key Swedish transport corridors, using consistent numeric thresholds and multiple performance metrics across diverse terrain, land cover, and deformation settings.

Both approaches capture consistent ground-motion patterns along all corridors, including known subsiding and climatically sensitive segments. The main difference lies in spatial sampling: PS+DS provides substantially higher point counts and improved corridor continuity, while EGMS-PS delivers a sparser, more conservative set. Critically, the higher PS+DS point count does not entail a systematic loss of precision, with comparable RMSE at corridor scale.

These findings emphasise that comparisons between operational and locally processed InSAR should not be read as strictly apple-to-apple, even under similar thresholds, they reflect different processing philosophies, each with distinct application implications. This directly answers the question posed at the outset: the two solutions are complementary rather than competing. For routine corridor screening, EGMS-PS is often sufficient, offering a harmonised baseline with a fast workflow, and PS+DS processing is warranted where denser sampling or sensitivity to localised motion in vegetated or non-urban terrain is required. The choice should be guided by the monitoring objective rather than an assumption that either approach is universally superior.

Code and data availability

The source code associated with this study is publicly available as a versioned repository archived on Zenodo at https://doi.org/10.5281/zenodo.19958548 (Aminjafari, 2026).

The Copernicus Sentinel-1 SAR images can be downloaded from https://asf.alaska.edu. The 30-m Copernicus Global and European Digital Elevation Model can be downloaded from https://dataspace.copernicus.eu/explore-data/data-collections/copernicus-contributing-missions/collections-description/COP-DEM. The EGMS-PS Calibrated product can be downloaded from the EGMS platform https://egms.land.copernicus.eu/. The 10-m resolution Swedish National Land Cover

https://doi.org/10.5194/egusphere-2026-3758
Preprint. Discussion started: 20 August 2026

Database can be downloaded from https://www.naturvardsverket.se/en/services-and-permits/maps-and-map-services/national-land-cover-database/. The MiaPlPy and SARvey packages are available at https://github.com/insarlab/MiaplPy and https://github.com/luhipi/sarvey respectively.

Author contributions

SA conceptualised the study, processed and analysed the data, produced the figures, and prepared the original draft. FN, MD, and LEBE acquired funding and, together with FC, contributed to the conceptualisation, methodology, and validation. FN and LEBE supervised the work. All co-authors reviewed and edited the manuscript and approved the final version.

Competing interests

The authors declare that they have no conflict of interest.

Acknowledgements

During the preparation of this work the authors used OpenAI ChatGPT to support language editing and code development. All scientific analysis, interpretation of results, and conclusions were performed by the authors, who take full responsibility for the content of the manuscript.

Financial support

This work was supported by the Swedish Transport Administration (Trafikverket), with project number: TRV 2023/14721, and case-ID: 7767, as well as by the Swedish National Space Agency (Rymdstyrelsen) with project number: 2024-00166.

References

Aminjafari, S.: EGMS vs PS-DS Phase-linking [software], https://doi.org/10.5281/zenodo.19958548, 2026.

Aminjafari, S., Brown, I. A., and Jaramillo, F.: Evaluating D-InSAR performance to detect small water level fluctuations in two small lakes in Sweden, Environ. Res. Commun., 6, 091006, https://doi.org/10.1088/2515-7620/ad7701, 2024.

Ansari, H., De Zan, F., and Bamler, R.: Sequential Estimator: Toward Efficient InSAR Time Series Analysis, IEEE Trans. Geosci. Remote Sensing, 55, 5637–5652, https://doi.org/10.1109/TGRS.2017.2711037, 2017.

Ansari, H., De Zan, F., and Bamler, R.: Efficient Phase Estimation for Interferogram Stacks, IEEE Trans. Geosci. Remote Sensing, 56, 4109–4125, https://doi.org/10.1109/TGRS.2018.2826045, 2018.

https://doi.org/10.5194/egusphere-2026-3758
Preprint. Discussion started: 20 August 2026

Azadnejad, S., Hrysiewicz, A., Trafford, A., O'Loughlin, F., Holohan, E. P., Kelly, F., and Donohue, S.: InSAR supported by geophysical and geotechnical information constrains two-dimensional motion of a railway embankment constructed on peat, Engineering Geology, 333, 107493, https://doi.org/10.1016/j.enggeo.2024.107493, 2024.

Azadnejad, S., Kandiri, A., Hrysiewicz, A., O'Loughlin, F., Holohan, E. P., Dev, S., and Donohue, S.: Application of deep learning for coherent pixel selection in time series InSAR for urban area and transport infrastructure monitoring, International Journal of Applied Earth Observation and Geoinformation, 142, 104718, https://doi.org/10.1016/j.jag.2025.104718, 2025.

Aziz Zanjani, F., Amelung, F., Piter, A., Sobhan, K., Tavakkoliestahbanati, A., Eberli, G. P., Haghighi, M. H., Motagh, M., Milillo, P., Mirzaee, S., Nanni, A., and Andiroglu, E.: InSAR Observations of Construction-Induced Coastal Subsidence on Miami's Barrier Islands, Florida, Earth and Space Science, 11, e2024EA003852, https://doi.org/10.1029/2024EA003852, 2024.

Banic, M., Ristic-Durrant, D., Madic, M., Klapper, A., Trifunovic, M., Simonovic, M., and Fischer, S.: The Use of Earth Observation Data for Railway Infrastructure Monitoring—A Review, Infrastructures, 10, 66, https://doi.org/10.3390/infrastructures10030066, 2025.

Berardino, P., Fornaro, G., Lanari, R., and Sansosti, E.: A new algorithm for surface deformation monitoring based on small baseline differential SAR interferograms, IEEE Trans. Geosci. Remote Sensing, 40, 2375–2383, https://doi.org/10.1109/TGRS.2002.803792, 2002.

Costantini, M., Minati, F., Trillo, F., Ferretti, A., Novali, F., Passera, E., Dehls, J., Larsen, Y., Marinkovic, P., Eineder, M., Brcic, R., Siegmund, R., Kotzerke, P., Probeck, M., Kenyeres, A., Proietti, S., Solari, L., and Andersen, H. S.: European Ground Motion Service (EGMS), in: 2021 IEEE International Geoscience and Remote Sensing Symposium IGARSS, 2021 IEEE International Geoscience and Remote Sensing Symposium IGARSS, 3293–3296, https://doi.org/10.1109/IGARSS47720.2021.9553562, 2021.

Crosetto, M., Solari, L., Balasis-Levinsen, J., Bateson, L., Casagli, N., Frei, M., Oyen, A., Moldestad, D. A., and Mróz, M.: Deformation Monitoring at European Scale: The COPERNICUS Ground Motion Service, The International Archives of the Photogrammetry, Remote Sensing and Spatial Information Sciences, XLIII-B3-2021, 141–146, https://doi.org/10.5194/isprs-archives-XLIII-B3-2021-141-2021, 2021.

Crosetto, M., Cuevas-González, M., Mróz, M., Moldestad, D. A., Raspini, F., Casagli, N., Bateson, L., Novellino, A., Motagh, M., Guerrieri, L., and Comerci, V.: European Ground Motion Service: A decade of Sentinel-1 observations, Remote Sensing of Environment, 339, 115389, https://doi.org/10.1016/j.rse.2026.115389, 2026.

Copernicus DEM - Global and European Digital Elevation Model | Copernicus Data Space Ecosystem: https://doi.org/10.5270/ESA-c5d3d65, last access: 9 December 2025.

Ferretti, A., Prati, C., and Rocca, F.: Permanent scatterers in SAR interferometry, IEEE Trans. Geosci. Remote Sensing, 39, 8–20, https://doi.org/10.1109/36.898661, 2001.

Ferretti, A., Fumagalli, A., Novali, F., Prati, C., Rocca, F., and Rucci, A.: A New Algorithm for Processing Interferometric Data-Stacks: SqueeSAR, IEEE Trans. Geosci. Remote Sensing, 49, 3460–3470, https://doi.org/10.1109/TGRS.2011.2124465, 2011.

Ferretti, A., Passera, E., and Capes, R.: End-to-end implementation and operation of the European Ground Motion Service (EGMS): Algorithm Theoretical Basis Document, 2025.

https://doi.org/10.5194/egusphere-2026-3758
Preprint. Discussion started: 20 August 2026

Johnsson, I. and Balstrøm, T.: A GIS-based screening method to identify climate change-related threats on road networks: A case study from Sweden, Climate Risk Management, 33, 100344, https://doi.org/10.1016/j.crm.2021.100344, 2021.

Karami, E., Shami, S., Maghsoudi, Y., Ranjgar, B., and Azadnejad, S.: Investigating the InSAR Phase Bias in the SBAS Algorithm and Its Effect on Different Landcovers, IEEE Access, 13, 82514–82526, https://doi.org/10.1109/ACCESS.2025.3568144, 2025.

Koks, E. E., Rozenberg, J., Zorn, C., Tariverdi, M., Vousdoukas, M., Fraser, S. A., Hall, J. W., and Hallegatte, S.: A global multi-hazard risk analysis of road and railway infrastructure assets, Nat Commun, 10, 2677, https://doi.org/10.1038/s41467-019-10442-3, 2019.

Kotzerke, P., Siegmund, R., and Langenwalter, J.: End-to-end implementation and operation ofthe European Ground Motion Service(EGMS): Product User Manual, 2022.

Li, G., Törnqvist, T. E., and Chen, J.: Evaluating InSAR-derived rates of surface-elevation change along the central U.S. Gulf Coast, Earth Observation, 1, 1–13, https://doi.org/10.5194/eo-1-1-2026, 2026.

Mirzaee, S., Amelung, F., and Fattahi, H.: Non-linear phase linking using joined distributed and persistent scatterers, Computers & Geosciences, 171, 105291, https://doi.org/10.1016/j.cageo.2022.105291, 2023.

Piter, A., Haghshenas Haghighi, M., and Motagh, M.: Challenges and Opportunities of Sentinel-1 InSAR for Transport Infrastructure Monitoring, PFG, 92, 609–627, https://doi.org/10.1007/s41064-024-00314-x, 2024.

Sadhasivam, N., Ohenhen, L., Khorrami, M., Werth, S., and Shirzaei, M.: Building damage risk in sinking Indian megacities, Nat Sustain, 1–13, https://doi.org/10.1038/s41893-025-01663-0, 2025.

SHK: Derailment of a passenger train (Report), Swedish Accident Investigation, Sweden, 2024.

SHK: Derailment of freight train no 9914 at Malmbanan (Report), Swedish Accident Investigation, Sweden, 2025a.

SHK: Landslide in Stenungsund (Report), Swedish Accident Investigation, Sweden, 2025b.

Staniewicz, S., Mirzaee, S., Fattahi, H., Oliver-Cabrera, T., Havazli, E., Gunter, G., Jeon, S.-Y., Bato, M. G., Kim, J., Sangha, S. S., Chapman, B., Handwerger, A. L., Govorcin, M., Agram, P., and Bekaert, D.: Near-Real-Time InSAR Phase Estimation for Large-Scale Surface Displacement Monitoring, https://doi.org/10.48550/ARXIV.2511.12051, 2025.

Staniewicz, S. J., Mirzaee, S., Gunter, G. M., Oliver-Cabrera, T., Havazli, E., and Fattahi, H.: Dolphin: A Python package for large-scale InSAR PS/DSprocessing, JOSS, 9, 6997, https://doi.org/10.21105/joss.06997, 2024.

Wu, S., Zhang, B., Li, Y., Xiong, S., and Ding, X.: Comparative analysis of PS-InSAR and DS-InSAR for deformation monitoring of transportation infrastructure in Greater Bay Area, China, Remote Sensing Applications: Society and Environment, 41, 101872, https://doi.org/10.1016/j.rsase.2026.101872, 2026.

Yang, Y., Liu, Y., Guo, Y., Shen, J., Xie, C., Zhang, N., Tian, B., Zhu, Y., and Mao, Y.: An InSAR-Based Framework for Advanced Large-Scale Failure Probability Assessment of Oil and Gas Pipelines, Remote Sensing, 17, 504, https://doi.org/10.3390/rs17030504, 2025.

Yunjun, Z., Fattahi, H., and Amelung, F.: Small baseline InSAR time series analysis: Unwrapping error correction and noise reduction, Computers & Geosciences, 133, 104331, https://doi.org/10.1016/j.cageo.2019.104331, 2019.